

## ECV DOPING PROFILE MEASUREMENTS OF ALUMINIUM ALLOYED BACK SURFACE FIELDS

F. Huster and G. Schubert  
University of Konstanz, Department of Physics, 78457 Konstanz, Germany  
email: frank.huster@uni-konstanz.de

**ABSTRACT:** A comprehensive study of the doping profiles of aluminium alloyed (screen printed and RTP fired) back surface field (BSF) layers in crystalline silicon is presented, based on the electrochemical capacitance-voltage (ECV) profile measuring technique combined with an advanced evaluation. Precise measurements of pure Al profiles are compared with simulations made using the Al-Si phase diagram. The contribution of boron doping from the glass frit and the dependence of BSF formation on crystal orientation investigated. The importance of incomplete ionization of Al atoms at room temperature is introduced.

**Keywords:** Aluminium, Back Surface Field, Doping Profile

### 1 INTRODUCTION

“Carrier profile engineering” is needed to further optimize the properties of the aluminium alloyed back surface field beyond the usual empirical approach. The electrical properties of the BSF are determined by the doping level, the doping profile, lateral inhomogeneities and defects. The first three issues are addressed in this work. The results are intended to provide new knowledge and tools for profile engineering and thereby help to close the gap between actual and theoretical best BSF performance.

The ECV (electrochemical capacitance voltage) technique is well suited for carrier profile measurements. When applied with care and advanced evaluation procedures as described in sections 3 to 5, profile measurements with a high absolute accuracy can be obtained.

### 2 EXPERIMENTAL

The four screen printable Al pastes listed in Table I were used. They were printed onto polished FZ silicon and fired in an RTP furnace for BSF formation. The exact paste compositions are not disclosed by the paste manufacturers. The frit contents are estimated from safety data sheets and the results found in this work. Pastes A and D are not commercially available.

Paste		Assumed glass frit content	Boron?
A	“pure” Al	Very low	Very low
B	Ferro 53-038	Medium	In glass frit
C	DuPont PV331	High	In glass frit
D	Al +3% B	Medium	3% added

**Table I:** Al pastes used in this work. The content of lead borosilicate glass is in the range of a few wt-%.

The ECV measurements were performed using an Accent PN4300PC profiler. The measurement spot was defined by a sealing ring of 3.5 mm in diameter. The electrolyte used was 0.1 M NaH<sub>2</sub>F<sub>2</sub> solution and an effective dissolution valence of  $z = 3.7$  was assumed. For details on the measurement technique see [1] and references therein.

### 3 EVALUATION OF ECV MEASUREMENTS

To obtain a “real” concentration profile from an ECV measurement, corrections for several effects have to be made. A program was therefore developed by which ECV measurements of BSF profiles can be simulated on the basis of a tentative real profile (or a lateral profile distribution, see section 4). By fitting this simulation to the measurement, the real profile can be obtained. The following effects are taken into account:

- Surface roughness: The wavy surface of an alloyed BSF has an area larger than a planar surface by a factor of 1.01 to 1.1. The measured concentration is proportional to the square of this enlargement factor.
- The walls of the etch crater contribute significantly to the measured capacitance for measurements deeper than several  $\mu\text{m}$ . A functional dependence of the wall area on the crater depth was found empirically. The calculated edge effect fits well to the measured effect, as shown in Figure 1.

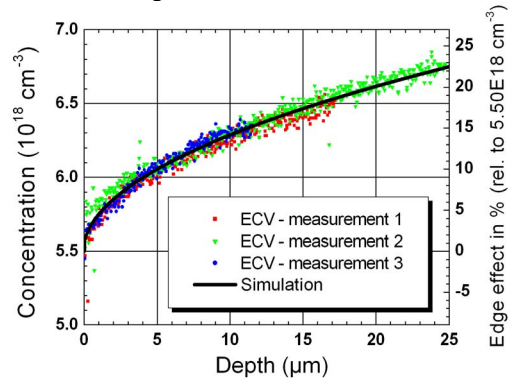


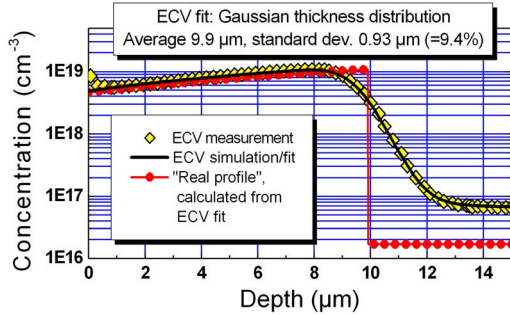
**Figure 1:** Edge effect (contribution of etch crater walls) as measured on a uniformly doped wafer. Note that the effect amounts to 10% in the depth range of a typical Al BSF (see scale on the right).

- Different doping levels present on the silicon surface (due to the doping gradient the walls and the crater bottom are differently doped and due to thickness inhomogeneities in the BSF there is a lateral distribution of doping levels on the crater bottom), lead to a signal averaging. It was found that the measured concentration is a generalized area weighted mean of order 0.5 of the concentration distribution. In case of two areas it is given by:

$$N_{ECV} = \left( \frac{A_1 \cdot \sqrt{N_1} + A_2 \cdot \sqrt{N_2}}{A_1 + A_2} \right)^2$$

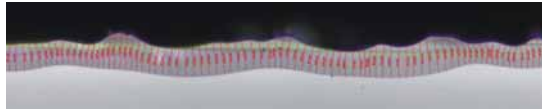
### BSF THICKNESS INHOMOGENEITY

Figure 2 shows a BSF profile measured using ECV, the simulated profile fitted to this result and the underlying real profile determined from the simulation. The rounded inner edge of the measured ECV profile can be modelled by assuming a Gaussian BSF thickness distribution and applying the mathematical procedures discussed in section 3.

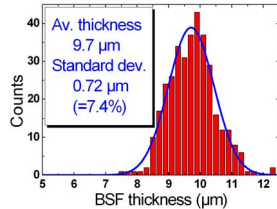


**Figure 2:** ECV measurement and profile simulation for the same sample as shown in Figure 3.

To verify this model, the thickness distribution of a BSF cross-section was measured by cleaving and staining in 1:3:6 (HF:HNO<sub>3</sub>:CH<sub>3</sub>COOH) etch. In Figure 3, this distribution and a Gaussian fit for a sample fired at 825°C for 1 s (13.4 mg/cm<sup>2</sup> Al, paste B) is shown. This is the same sample for which the ECV measurement is shown in Figure 2.



**Figure 3a,3b:** Direct measurement of the BSF thickness distribution using optical microscope pictures of BSF cross-sections. A Gaussian distribution is fitted to the measurements.



Because the thickness inhomogeneities on a lateral scale are much smaller than the size of the measurement spot, an effective averaging is included in the ECV measurements. Taking into account the corrections listed in section 3, an ECV profile can be calculated and fitted to the measurement, here with the BSF thickness and standard deviation as fitting parameters. There are two significant results: Firstly, the calculated curve fits well to the measurement, yielding a Gaussian distribution in good agreement with that obtained from a direct thickness measurement (Figure 3). Secondly, a real concentration profile is obtained, representing that which would have been measured without thickness inhomogeneities and without measurement technique related effects. The local BSF profiles are assumed to have the shape of this real profile, only differing in depth according to the Gaussian distribution.

The ECV measurement technique combined with this evaluation procedure is therefore able to quantify the thickness inhomogeneities of an alloyed BSF. In Table II optical microscope pictures of three BSF profiles are shown. The thickness inhomogeneity and the surface

roughness are considerably reduced by using a larger amount of deposited aluminium. Interestingly the BSF thickness seems to saturate at about 10 μm on (100) oriented silicon using standard firing parameters.

Al (mg/cm <sup>2</sup> )	BSF thickness (from ECV)	
	Average (μm)	Gauss.stand.dev. %
	5.9	20.0
	13.4	9.4
	28.1	5.0

**Table II:** Optical microscope pictures of Al-BSF cross-sections. Paste B, fired at 825°C for 1 s, ramp up and down by 20 K/s. Substrate: polished (100) FZ silicon.

### 4 WHAT IS ACTUALLY MEASURED BY ECV?

In the doping range of 10<sup>17</sup> to 10<sup>19</sup> cm<sup>-3</sup>, incomplete ionization of dopant atoms is present even at room temperature. This interesting, yet often neglected effect [2, 3], is especially important for investigations of Al BSFs since the Al doping concentration lies in the relevant range and the higher ionization energy of Al compared to shallow dopants like B (69 meV to 44 meV) causes a large effect. As neither experimental investigations nor calculations of incomplete ionization in Al doped silicon were found in the literature, calculations were done to estimate the relevance of this effect for the Al BSF. The results are shown in Figure 4 and should be read as qualitative as the physics of highly doped silicon is involved and still a topic of fundamental solid state research. It is expected from this calculation that 20 to 50% of the substitutional Al atoms do not contribute to the hole concentration.

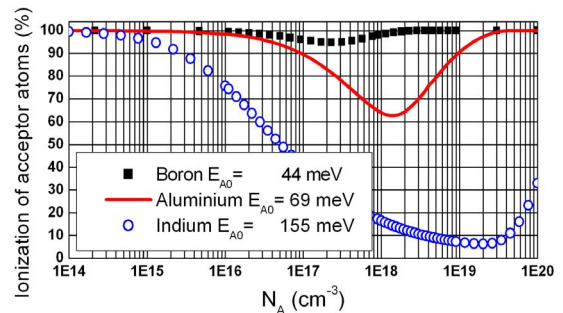


**Figure 4:** Calculated fraction of ionized substitutional dopant atoms at 300 K. At low concentrations and also at high concentrations above the metal-insulator(MI)-transition the atoms are fully ionized. The doping range of the MI-transition for Al and In is not well known.

In view of the incomplete ionization, it is important to clarify what concentration is measured by capacitance-voltage techniques. The concentration is determined by measuring the differential capacity on varying the reverse biased voltage across a rectifying junction. The band bending (or equivalently the high electric field) in the depletion region leads to a complete ionization of the dopant atoms [4]. Therefore by the ECV technique the

concentration of all substitutional Al atoms is measured. For the solar cell operation the carrier profile is important, which is lower according to the degree of incomplete ionization.

The effect of incomplete ionization should appear as a difference in the measured BSF sheet resistance and that calculated from an ECV profile. Results for the 4 pastes investigated in this work are shown in Table III.

BSF made from paste ...	Sheet resistance (Ohm/sq)	
	Measured (4 PP)	Calculated from ECV profile
A ("pure" Al)	25.3	15.0
B (B in glass frit)	11.0	8.7
C (B in glass frit)	3.0	2.7
D (B added)	2.7	2.7

**Table III:** Comparison of BSF sheet resistances obtained directly and from ECV profiles. As expected, with a pure Al paste, the effect of incomplete ionization appears to be significant.

While for the profiles that are dominated by boron doping (pastes B, C, and D) a good agreement is found (i.e., the concentration of holes determining the sheet resistance is close to the concentration of dopant atoms as measured by ECV), the difference in case of the BSF profile of paste A is consistent with an average ionization degree of 60%. More work has to be done to clarify this effect.

## 5 DOPING PROFILES OF "PURE" AL PASTE

Precise measurements of (almost) pure Al BSF doping profiles made from paste A and fired at different peak temperatures are shown in Figure 5 to provide reliable data for solar cell simulations. While the liquidus curve of the binary Al-Si phase diagram is well known, large discrepancies in the Si solidus curve determining the Al solid solubility still exist in the literature [5, 6]. The stars in Figure 5 show a profile calculated using recently published solubility data [7].

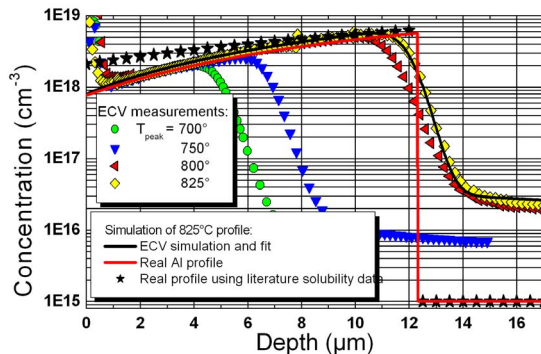


**Figure 5:** ECV profile of "pure" aluminium BSFs made from paste A (Al: 20 mg/cm<sup>2</sup>) on polished (100) FZ silicon. Firing was done in an RTP furnace for 3 s at  $T_{\text{peak}}$ . The origin of the steep structure on the left side (at the BSF surface) has not yet been clarified.

The close agreement between the measured and simulated profiles shown in Figure 5 indicates that on (100) oriented silicon the BSF formation is determined by equilibrium thermodynamics according to the phase diagram. The maximum Al concentration obtained in a

typical contact firing process with  $T_{\text{peak}} = 825^\circ\text{C}$  is between  $5$  and  $7 \times 10^{18} \text{ cm}^{-3}$ . The surface concentration for all profiles is uncertain:  $8 \times 10^{17} \text{ cm}^{-3}$  extrapolated from the measurements,  $2 \times 10^{18} \text{ cm}^{-3}$  according to [7], or close to  $10^{19} \text{ cm}^{-3}$ , if the surface peak in Figure 5 is not a measurement artifact.

## 6 PROFILES OF FRITTED AL AND AL+B PASTES

The ECV profiles of BSFs made from pastes B to D are similar in shape to the "pure Al" profile of paste A, but on a higher doping level as shown in Figure 6. SIMS measurements (unfortunately not well calibrated in doping level and depth) reveal the importance of boron doping in these cases. Boron is incorporated into the silicon lattice in the same way as Al, i.e. according to its (higher) solid solubility. Paste D (with intentional boron addition) and paste C (probably with high frit content) provide enough boron to reach concentrations in the range of  $5 \times 10^{19} \text{ cm}^{-3}$ . Paste B with medium frit content probably contains less boron, therefore saturation is not reached and the doping concentration is partly determined by the segregation of boron during epitaxial BSF growth. The occurrence of substantial boron doping when using standard fritted Al pastes (probably without intentional boron addition) might be caused by a reduction of the borosilicate glass during alloying. The observations are consistent with the differing (1-10 wt-%) amount of glass frits in the pastes.

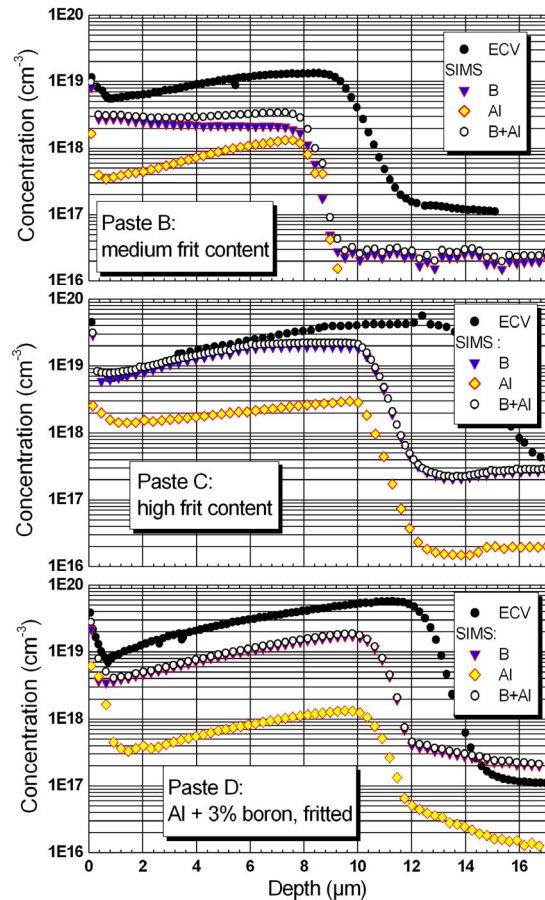


**Figure 6:** ECV and SIMS (not calibrated) measurements of BSF doping profiles. All samples were polished (100) FZ silicon, fired at  $825^\circ\text{C}$  for 1 s. Different amounts of deposited Al paste.

## 7 DEPENDENCE ON CRYSTAL ORIENTATION

Surprisingly, on (111) oriented silicon a totally different ECV profile was measured, showing a much higher Al concentration than on (100) silicon (Figure 7). Additionally, the deep (>10 μm) doping profile was found to *increase* towards the surface up to very high concentrations, by far exceeding the aluminium solid solubility in silicon. Obviously the incorporation of the Al is in this case no longer governed by equilibrium thermodynamics as described by the binary phase diagram but by kinetics during epitaxial growth. Only few investigations of solute trapping have been found in literature (see for instance [8] for Ga in Si). The resulting profile provides a drift field which is in principle well suited for a good BSF performance by driving the minority carriers away from the surface, but unfortunately the doping level is slightly too high (doping levels above 10<sup>19</sup> cm<sup>-3</sup> lead to a low τ<sub>eff</sub> in the BSF due to Auger recombination and a significant free carrier absorption).

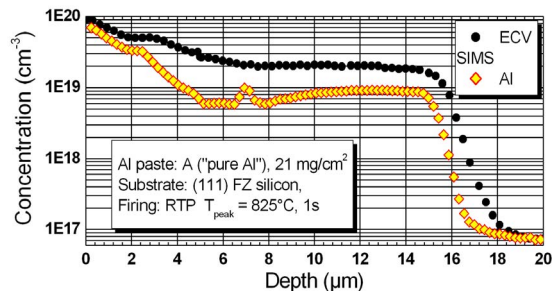


**Figure 7:** ECV and SIMS profiles of Al BSF made using paste A on (111) oriented FZ silicon, showing concentrations much higher than the Al solid solubility.

In Figure 8, the BSF sheet resistance vs. the etch removal (i.e. etching rate) in hot NaOH is shown for Cz wafers of (100) and (111) orientation and for individual crystallites of mc-Si wafers. The etching rates of (100) and (111) oriented Cz silicon are related by a ratio of 2.5:1<sup>1</sup>. Solute trapping leads to a sheet resistance of the (111) Cz that is four times lower than that of the (100) oriented Cz. If the (111) plane is slightly misoriented (by a few degrees), the solute trapping effect is drastically diminished. The mc-Si grains show a broad range of etch removal depending on crystallite orientation, obviously correlated with a distribution of BSF sheet resistance.

To explain this effect, the following model is proposed. The anisotropic alkaline etch creates a rough surface mainly composed of slowly etched (111) facets. The fraction of (111) oriented facets depends on the crystal orientation of the individual mc-Si grains<sup>2</sup>. Both the etch rate in NaOH as well as the BSF sheet resistance are a local average of the contributions by (111) and other facets. The BSF sheet resistance and the etching rate are both assumed to be lower the more (111) facets

<sup>1</sup> The literature value for the ratio of (100) to (111) etching rates, far above 100, is only reached in well controlled experiments. Usually the attack of the etchant at the edges of the non perfect surface leads to a much lower anisotropy, as it is seen here.

<sup>2</sup> For example, on (100) oriented grains truncated pyramids are formed with (111) side walls and a (100) ceiling.

are present. These results imply variable BSF passivation properties, depending on the grain orientation of mc Si.

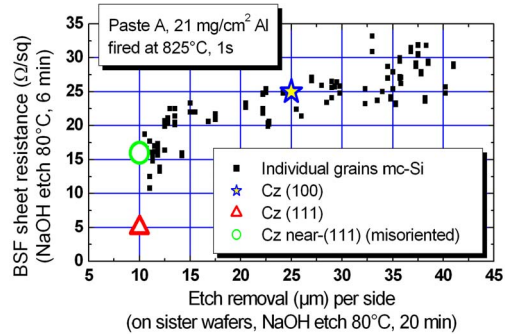


**Figure 8:** BSF sheet resistance dependence on crystal orientation. In a first experiment, the etch removal in a 20 min NaOH etch was determined by mechanical thickness measurements to classify the individual grains on mc wafers and the Cz wafers by their etching rate, shown on the x-axis. In a subsequent experiment, BSFs were formed on sister wafers (subjected to a standard 6 min NaOH saw damage removal) and the resulting sheet resistances were measured with a 4 point probe (y-axis). A correlation of slow etching rates (probably with a large fraction of (111)-oriented facets) and low BSF sheet resistances is evident.

## 8 SUMMARY AND CONCLUSIONS

The ECV technique, combined with an advanced evaluation software, proved to be a powerful tool for BSF investigations. The aluminium profiles on (100) silicon match well the calculations based on the phase diagram. For solar cells, the effect of boron doping from the glass frit and the (111) solute trapping of aluminium are particularly important. First investigations show that incomplete ionization appears to be significant Al doped silicon and therefore it would be useful to more precisely investigate this effect.

The results provide a basis for further optimization of Al BSFs. An important issue to be covered in future work is the amount of crystal defects and impurities introduced during BSF formation.

### Acknowledgements

The authors gratefully acknowledge the financial support of the EC under project N<sup>o</sup> ENK6-CT-2001-00560 (EC2Contact) and project N<sup>o</sup> ENK6-CT-2002-00666 (TOPSICLE) and would like to thank Radovan Kopecek and Bernhard Fischer for fruitful discussions. Part of the work for this paper was supported with funding of the German BMU under contract number 0329844F (OPTIMAN). The content of this publication is the responsibility of the authors.

### References

- [1] E. Peiner, J.Electrochem.Soc. **142** (1995) 576
- [2] P.P. Altermatt, this conference
- [3] Y.V. Mamontov, IEICE Trans.El **E77-C** (1994) 287
- [4] T.J. Woodley, Solid-State El. **20** (1977) 385
- [5] F.A. Trumbore, Bell System Tech. J. **39** (1960) 205
- [6] J.L. Murray, Bull. of Alloy Phase Diagr. **5** (1984) 74
- [7] T. Yoshikawa, J.Electrochem.Soc. **150** (2003) G465
- [8] B.E. Summer, J.Electrochem.Soc. **125** (1978) 1817.